Journal of Structural Geology, Vol. 8, No. 8, pp. 897 to 909, 1986
Printed in Great Britain

0191-8141/86 $03.00 + 0.00
Pergamon Journals Ltd.

The relationship between the geometry of normal faults and that of the sedimentary layers in their hanging walls

N. J. WHITE, J. A. JACKSON and D. P. MCKENZIE

Bullard Laboratories, Madingley Road, Cambridge CB3 0EZ, U.K.

(*Received* 7 *August* 1985; *accepted in revised form* 30 *January* 1986)

Abstract—We derive an analytical expression that relates the shape of a fault in cross-section to the shape of the bedding horizons in its hanging wall block. The expression assumes that the hanging wall deforms by simple shear and that the footwall remains undeformed throughout. Although this paper concentrates on normal faults, the expression is equally valid and applicable to thrust faults. The direction of simple shear in the hanging wall block is arbitrary and has a dramatic effect on the predicted fault or bedding geometry. There is no reason to believe that the simple shear occurs on vertical planes, as is commonly assumed in graphical approaches to this problem, and ignoring the presence of inclined simple shear is likely to lead to considerable underestimates of the amount of extension across normal faults and in the amount of shortening across thrusts. Similar though more complicated expressions can be obtained when compaction within the hanging wall block is taken into account. For a planar normal fault such compaction may result in the development of a hanging wall syncline.

INTRODUCTION

IN REGIONS of extensional tectonics, a knowledge of the geometry and kinematics of large-scale faults is obviously of crucial importance, not only in evaluating particular commercial prospects, but also in understanding the nature and amount of extension involved. Although it is now clear that large-scale crustal and lithospheric stretching occurred during the formation of many continental sedimentary basins and margins, it is not always easy to reconcile estimates of the amount of stretching obtained from measurements of crustal thickness and subsidence with those obtained from the observed normal faulting (e.g. de Charpal *et al.* 1978, Le Pichon & Sibuet 1981, Wood & Barton 1983, Ziegler 1983). Much of this disagreement is probably attributable to a poor understanding of the geometry of the large normal faults that accommodate at least some, and perhaps most, of the extension at shallow crustal levels.

Recent reviews have tended to concentrate on observations of the faults themselves, using either outcrops and seismic reflection profiles (e.g. Wernicke & Burchfiel 1982, Anderson *et al.* 1983, Smith & Bruhn 1984) or seismological observations of earthquakes generated by active normal faults (e.g. Jackson & McKenzie 1983, Jackson 1986). This paper is concerned with a different approach to the same problem: what is the detailed relationship between the geometry of a normal fault and the geometry of the sediments in its hanging wall? The usual method of investigating their connection is graphical (Verrall 1981, Gibbs 1983, 1984) and assumes that the hanging wall is deformed by simple shear in vertical planes. We develop below a general analytic solution to the same problem. Our solution also assumes the deformation is by simple shear, but makes no assumption about the inclination of the shear planes to the vertical.

RELATIONS BETWEEN SEDIMENT AND FAULT GEOMETRIES

The problem

The problem is illustrated by Fig. 1, showing a listric normal fault that, for simplicity, becomes planar and horizontal at depth. (In general, faults need do neither of these things.) The geometry before movement is shown in Fig. 1(a). If movement now occurs such that all points in the hanging wall move a vector **h** relative to the footwall, the geometry would look like Fig. 1(b). In this

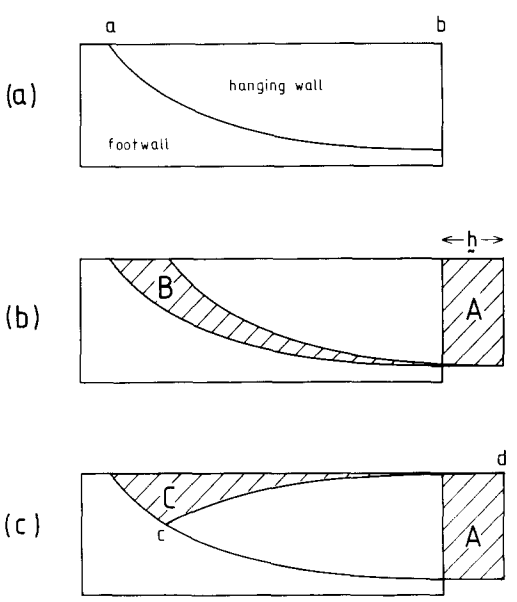

Fig. 1. Diagrams to illustrate the deformation of the hanging wall necessary to fill the potential void beneath it, if it moves a vector **h** relative to the footwall. After internal deformation of the hanging wall only points far from the fault outcrop have a displacement **h** relative to the footwall. Note that the footwall remains undeformed.

case **h** is horizontal with magnitude h. The cross-section has extended by area A, which, if there is no movement out of the plane of the section, is equal to area B. In reality no voids will occur and the hanging wall deforms, filling the gap beneath it, to leave a space above (Fig. 1c), such that area C = area A = area B. It is clear that the shape of the hanging wall surface (or 'rollover') in Fig. 1(c) is in some way related to the underlying fault geometry. Only at some remote point in the hanging wall, far from the surface outcrop of the fault, will the relative movement between hanging wall and footwall be represented by **h**. Closer to the fault outcrop the relative motion has been changed by the internal deformation of the hanging wall necessary to fill the (potential) void beneath it. A cross-section in which the areas A, B and C are equal is sometimes said to be 'balanced' (e.g. Gibbs 1983), though it is important to realize that this only refers to the preservation of hanging wall cross-sectional area during movement. A more powerful constraint is imposed by the use of this term in Dahlstrom's (1969) sense, in which bed length is preserved during movement. This sense is not applicable here, as the length ab in Fig. 1(a) is not equal to the length cd in Fig. 1(c).

The hanging wall cross-sectional area is preserved in Fig. 1, and it is possible to describe the change in its shape by simple shear in the plane of section. The graphical techniques used by Verrall (1981) and Gibbs (1983, 1984) to relate the fault and rollover geometries assume that the simple shear occurs on vertical planes. However, there is no reaon why this should be so, and indeed, antithetic faults observed within hanging wall blocks are generally not vertical. We will now develop more general analytical relations between fault and sediment geometries, that allow for non-vertical simple shear.

Note that the footwall in Fig. 1 remains undeformed throughout. This is an important assumption for both graphical and analytical methods, and will be discussed later.

The forward problem: from fault to sediment geometry

To begin with we will consider the movement in a coordinate frame attached to the footwall block. The planes in which simple shear occurs are parallel to the y' direction, which is not, in general, perpendicular to the Earth's surface (Fig. 2). In this frame, the velocity in the x' direction is a constant U_0 and that in the y' direction is $v = v(x')$. The shape of the bed is $B' = B'(x')$ and that of the fault is $F' = F'(x')$, where B' and F' are the y' coordinates of the bed and the fault.

Consider an element of bed ab whose length in the x' direction is $\delta x'$, which has been moved a small distance $U_0\,\delta t$ in the x' direction and then deformed by simple shear parallel to the y' direction, such that point a moves to c and b moves to d. Let us suppose that before deformation the bed had a shape given by $R' = R'(x')$, with a dip of γ' at the point (x', y'). The coordinates of points a, b, c and d are

$$\begin{aligned} \text{a} &= (x', y') \\ \text{b} &= (x' + \delta x', y' + \delta x' \tan \gamma') \\ \text{c} &= (x' + U_0 \delta t, y' + v(x')\,\delta t) \\ \text{d} &= (x' + \delta x' + U_0\,\delta t, y' + \delta x' \tan \gamma' \\ &\quad + v(x' + \delta x')\,\delta t) \end{aligned}$$

The new dip of element cd is ψ', given by

$$\delta x' \tan \psi' = Ed = v(x' + \delta x')\,\delta t - v(x')\,\delta t + \delta x' \tan \gamma'$$

$$\therefore \tan \psi' = \frac{dv}{dx'} \cdot \delta t + \tan \gamma'. \tag{1}$$

However, if no voids are to form, the hanging wall must remain in contact with the fault surface, and the velocity at x' must always be parallel to the fault, of dip $\theta'(x')$

$$\therefore \frac{v}{U_0} = \tan \theta'$$

and

$$\frac{dv}{d\theta'} = \frac{U_0}{\cos^2 \theta'}. \tag{2}$$

Combining (1) and (2) gives

$$\tan \psi' = \frac{U_0\,\delta t}{\cos^2 \theta'} \frac{d\theta'}{dx'} + \tan \gamma'. \tag{3}$$

But $U_0\,\delta t$ is the displacement in the x' direction and constant throughout the hanging wall. If $U_0\,\delta t = h'$, then (3) may be rewritten

$$\tan \psi' - \tan \gamma' = h' \frac{d}{dx'} (\tan \theta') \tag{4}$$

or

$$\frac{d}{dx'} (B' - R') = h' \frac{d^2F'}{dx'^2}. \tag{5}$$

Hence integration gives

$$B' = h' \frac{dF'}{dx'} = R' + C', \tag{6}$$

where C' is a constant. This expression is only valid if

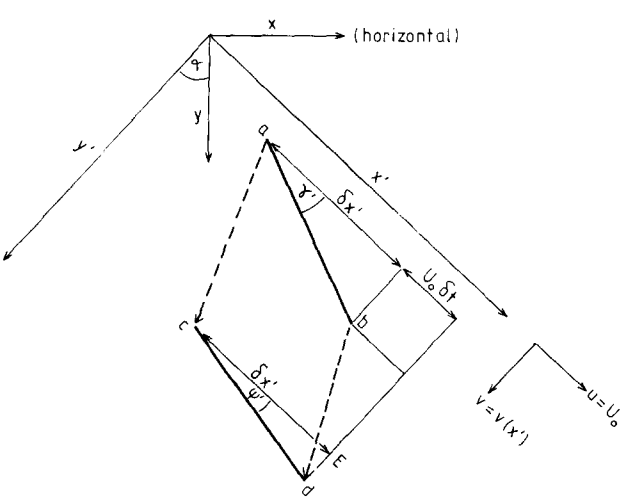

Fig. 2. Coordinate systems and geometrical relations used to derive the analytical expressions in the text.

dF'/dx' is continuous. In most cases the initial shape of the bed before deformation may simply be described by $R' = x' \tan \gamma_0' + D'$, where D' is a constant and γ_0' is the regional dip in the (x', y') frame. The value of C' depends on the origin chosen for the coordinate frame. If the origin is chosen such that $R' = R_0'$, $B' = B_0'$ and $dF'/dx' = \tan \theta_0'$ at $x' = 0$, then

$$C' = B_0' - R_0' - h' \tan \theta_0', \tag{7}$$

when (6) becomes

$$B' - B_0' = h'\left(\frac{dF'}{dx'} - \tan \theta_0'\right) + R' - R_0'. \tag{8}$$

These expressions are all in the (x', y') co-ordinate frame, in which simple shear is in the y' direction. But the (x', y') frame is rotated through an angle α with respect to the (x, y) frame, in which y is the downward pointing vertical (Fig. 2). Therefore the fault $F(x)$ and regional dip $R(x)$, defined in the (x, y) frame, must be rotated into the (x', y') frame using the relations

$$\begin{aligned} x' &= x \cos \alpha + y \sin \alpha \\ y' &= -x \sin \alpha + y \cos \alpha, \end{aligned} \tag{9}$$

where y is F or R. The heave h', must also be calculated in the (x', y') frame from the fault displacement vector before eqn (6) can be applied. A simple differentiation will then yield the geometry of the bedding in the hanging wall, B', in the (x', y') frame, which can be returned to the (x, y) frame using the relations

$$\begin{aligned} x &= x' \cos \alpha - y' \sin \alpha \\ y &= x' \sin \alpha + y' \cos \alpha. \end{aligned} \tag{10}$$

Equations (7) and (8) show that, given an observed fault geometry $F(x)$, the bedding in the hanging wall $B(x)$ may be determined if (i) the shape of the bed before movement, $R(x)$, (ii) the vector displacement on the fault, **h**, and (iii) the angle α between the downward vertical and the direction of simple shear in the hanging wall, are all specified. Note that the graphical constructions of Verrall (1981) and Gibbs (1983, 1984) assume that the simple shear is in vertical planes (i.e. $\alpha = 0°$). As will be shown later, this assumption greatly affects the predicted geometry of the hanging wall sediments.

The inverse problem: from sediment to fault geometry

From eqn (8)

$$F' = \frac{1}{h'} \int_0^{x'} \{B' - B_0' - (R' - R_0') + h' \tan \theta_0'\} \, dx', \tag{11}$$

where, once again, the boundary conditions B_0', θ_0' and h' must be known. Thus, given an observed bed geometry, the fault geometry may be calculated for various angles of simple shear, α. Because the inverse problem is an integration, it is more stable than the forward problem, which involves differentiation. This difference is fundamental and is not an artefact of the method used to solve the problem. Therefore the geometry of the beds in the hanging wall, determined by (8), will be strongly affected by small variations in the dip of the fault.

It is fortunate that the geologically important problem involves an integration, since numerical differentiation is not accurate, even when proper precautions are taken.

Assumptions

The main assumptions inherent in the derivation of equation (6) are:

(i) All displacements are small.

(ii) There is no movement out of the plane of section.

(iii) Deformation of the hanging wall is accomplished by simple shear. This is clear, since

$$\frac{\partial v}{\partial y'} = \frac{\partial u}{\partial x'} = \frac{\partial u}{\partial y'} = 0$$

and

$$\frac{\partial v}{\partial x'} = \frac{U_0}{h'} \cdot \frac{d}{dx'} (R' - B').$$

It is worth noting that simple shear on parallel planes is probably a reasonable assumption for the deformation in the hanging wall as it allows finite motion to occur on fault planes that do not intersect.

(iv) The footwall remains undeformed throughout.

(v) Sediment geometry has not been altered by compaction.

Of these, (iv) is probably the most important, and is least likely to be correct when applied to the deeper parts of faults that penetrate basement and are responsible for extension on a crustal scale. However, for growth faults of the type found in the Gulf of Mexico and Niger Delta, where extension of the basement does not take place, this assumption is more likely to be justified. Compaction may alter the geometry of beds within the hanging wall, particularly when syntectonic deposition occurs. A method which takes compaction effects into account is outlined in the Appendix.

On seismic reflection profiles the scales in the x and y directions are usually not equal. Provided that the exaggeration is constant (i.e. that the y scale is not a function of y), the expressions (6) and (7) will still be valid, and lead, of course, to corresponding exaggeration in the x and y scales of B and F. It is not therefore necessary to convert published seismic sections to true-scale sections; they can be digitized directly and the equations will then give the fault geometry at the same vertical exaggeration. Though this approach is clearly not accurate, it is often the only one possible (see below). However, unless **h** and α are accurately known, there is probably little purpose in making detailed corrections for velocity variations and compaction. If this is not done, it is important to remember that the value of α which should be used is the apparent, and not the true, dip of the planes of simple shear in the time section.

SYNTHETIC EXAMPLES

An analytic test

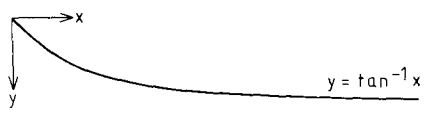

Fig. 3. The shape of a simple curved fault, given by $F = \tan^{-1} x$.

The use of the equations may be illustrated by a simple analytic example, with a fault shape described by $F = \tan^{-1} x$ (Fig. 3). Let us also assume that $R = 0$ and $\alpha = 0°$, in which case $x = x'$ and $y = y'$. Note that the dip of the fault is zero at $y = \pi/2$ and 45° at $y = 0$. From (6)

$$B = \frac{h}{1 + x^2} + C.$$

Since $B \to 0$ as $x \to \infty$, $C = 0$ and

$$B = \frac{h}{1 + x^2}. \tag{12}$$

Let us suppose the bed meets the fault at $h = x = \varepsilon$, where $\varepsilon \ll 1$. $(\varepsilon, \varepsilon)$ therefore satisfies both (12) and $y = \tan^{-1} x$.

Then

$$B = \frac{\varepsilon}{1 + x^2}. \tag{13}$$

The inverse problem can now be posed. Given equation (13) as the geometry of the bed, determine the fault geometry $F(x)$ if $\alpha = 0°$ and $R = 0$.

From (11)

$$F = \frac{1}{\varepsilon}\int_0^x \left(\frac{\varepsilon}{1 + x^2} + C\right) dx$$

$$= \tan^{-1} x + Cx + D. \tag{14}$$

Since the fault goes through the origin, $D = 0$. Clearly F is indeterminate unless dF/dx is given somewhere.

$$\frac{dF}{dx} = \frac{1}{1 + x^2} + C$$

If $dF/dx = 1$ at $x = 0$ (i.e. $\theta_0 = 45°$), then $C = 0$ and $F = \tan^{-1} x$, as it should.

The importance of inclined simple shear

The forward problem is illustrated in Fig. 4 using a fault with a dog-leg geometry, the two legs being joined by a circular arc. For simplicity $R = 0$. Two beds are drawn, both of which have the same infinitesimal displacement down the fault plane, and the same apparent horizontal heave on the fault, $h = \varepsilon$. However, in one case the hanging wall has been deformed by vertical simple shear ($\alpha = 0°$) and in the other case simple shear has occurred inclined at $\alpha = 45°$. The resulting shapes are very different, though as x becomes large, both return to the regional level of $R = 0$. Note that the displacement of the bed on the fault is the same in each

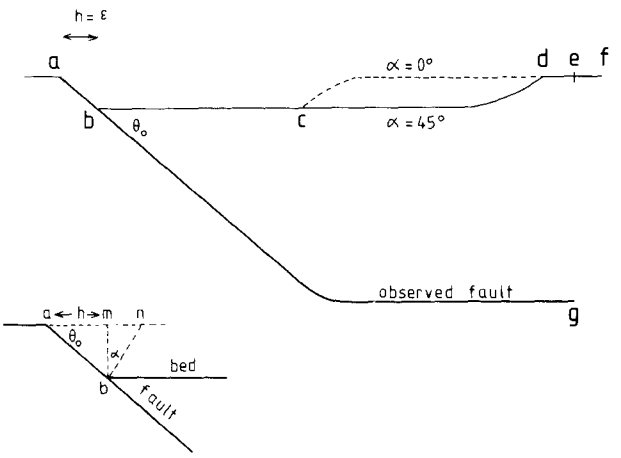

Fig. 4. Illustration of the forward problem using a dog-leg fault whose segments dipping at 45° and 0° are linked by the arc of a circle, so that dF/dx is continuous. The shape of the hanging wall surface is shown for simple shear at $\alpha = 0°$ (dashed) and $\alpha = 45°$ (solid line). The two surfaces are the same between b and c and d and f; although for $\alpha = 0°$ the final point on the fault, g, gives information on the bedding only as far as e. Equation (6) is only valid if ε is small, so the vertical scale of the hanging wall surface has been exaggerated arbitrarily to illustrate the difference between $\alpha = 0°$ and $\alpha = 45°$. The original level of the hanging wall surface is given by point a. The inset, bottom left, shows why, given a displacement ab on the fault with heave h, the horizontal movement of the rigid part of the hanging wall (i.e. overall mass transport or extension of the hanging wall block) depends on α. By referring to Fig. 1, it is clear that, for vertical simple shear point b has apparently come from m, and the horizontal extension is am = h. If the simple shear is inclined at α, point b has apparently come from n, and the horizontal extension is an = $h(1 + \tan\theta_0 \tan\alpha)$.

case, and that cross-sectional area is conserved. Why then is the area of the depression in each hanging wall different? The reason is that, in the case where $\alpha = 0°$, the horizontal displacement of the rigid part of the hanging wall is h, but where $\alpha \neq 0°$, the rigid part of the hanging wall is displaced $h(1 + \tan\theta_0 \tan\alpha)$. In this case, where $\theta_0 = 45°$ and $\alpha = 45°$, the inclined shear example represents an additional extra extension of 100%. If $\theta_0 = 60°$ and $\alpha = 60°$ this would rise to 300%. This example illustrates one of the most important results of this study: that the dip of the fault and the apparent displacement of a bed on it are not sufficient to work out the amount of extension, if that bed has also deformed in the hanging wall. The inclination of the simple shear in the hanging wall (perhaps given by the dip of minor antithetic faults) is also needed.

The inverse problem is illustrated in Fig. 5 using a bed whose shape is given by $B = h/(1 + x^2)$. Given $R = 0$,

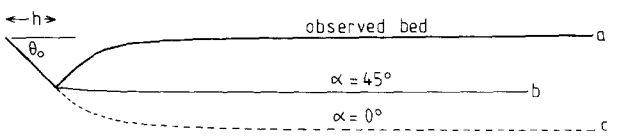

Fig. 5. Illustration of the inverse problem. Two different fault geometries are predicted from the same observed bed shape and apparent offset, h. The dashed line is the fault predicted for $\alpha = 0°$ and the solid line the fault predicted when $\alpha = 45°$. Note that when $\alpha = 45°$ the observed bed contains no information on the fault geometry beyond point b, whereas when $\alpha = 0°$ the fault may be extended as far as point c (vertically below a).

$\theta_0 = 45°$ and h, two different fault geometries are shown: one for $\alpha = 0°$ and the other for $\alpha = 45°$. These examples clearly illustrate the dramatic effect of inclined simple shear in the hanging wall block, and the danger of assuming $\alpha = 0°$.

Real examples and applications

The method described here should really be used only on seismic sections that are depth migrated and not affected by compaction. Unfortunately few such sections are available in the literature, and there are even fewer in which footwall and hanging wall stratigraphies are also shown, so that the heave, h, may be estimated. Nonetheless three examples that do not meet all these ideal requirements will now be briefly discussed. Differences between the results obtained below and those obtained using equations which deal with compaction (see Appendix) do not significantly alter our conclusions.

Predicting fault shapes or simple shear in the hanging wall

The first example is taken from Gans *et al.* (1985). Figure 6(a) shows a line drawing from a migrated seismic line across the Spring Valley in east-central Nevada. The alluvial fan and playa lake deposits that underlie Spring Valley define a wedge of west-dipping to sub-horizontal reflectors truncated on the west by a large normal fault (the Schell Creek Fault), which outcrops at the base of the Schell Creek Range. The seismic line runs approximately perpendicular to the strike of the Schell Creek Fault and motion is thought to be almost entirely in the plane of section.

Near the base of the layered sedimentary wedge, a prominent band of reflectors, labelled event E, may be traced. This event was identified as a disconformity between lacustrine sediments and underlying volcanic rocks by drill logs from the Yelland well (SP 1630). The dip of the Schell Creek Fault near the surface can be estimated as about 45° from the truncation of the layered reflectors in the hanging wall. This value is typical of other such faults in the Basin and Range Province (Smith & Bruhn 1984). Since the infilling sediments are predominantly lacustrine, we can assume that the regional dip at time of deposition was approximately horizontal, i.e. that $R = 0$. Can we now use the shape of horizon E to estimate the shape of the Schell Creek Fault at depth?

Figure 6(b) shows the shape of horizon E and the shape of the Schell Creek Fault beneath it, calculated using eqn (11), for two cases: one in which simple shear is vertical ($\alpha = 0°$) and the other in which it is inclined at 45° towards the west ($\alpha = 45°$). A minimum heave, h, is estimated from the truncated relectors as shown, $\theta_0 = 45°$ and $R = 0$. The two fault shapes are clearly very different. Interestingly, the shape calculated using $\alpha = 45°$ coincides at depth with reflectors labelled L in Fig. 6(a), which Gans *et al.* (1985) tentatively suggest may represent a deep part of the Schell Creek Fault. If this identification is correct it implies that $\alpha = 45°$ and the hanging wall is pervasively sheared by small faults dipping 45° towards the west. It is worth noting that Gans *et al.* identify a few such faults in their line drawing (Fig. 6a).

Although Fig. 6(a) is migrated, the y axis shows two way travel time rather than depth. The vertical exaggeration is unlikely to be uniform with depth, and, until the section is depth corrected, no firm conclusions can be drawn from this experiment. Nonetheless this example illustrates one use of the method: the main unknowns are the shape of the fault and the direction of simple shear, α. *A priori* knowledge of one of these (from reflections off the fault plane or observations of antithetic faulting in the hanging wall) could be used to predict the other.

Testing structural models

The second example is taken from Wernicke & Burchfiel (1982). Figure 7(a) shows an interpreted seismic section across a normal fault. Wernicke & Burchfiel (1982) also show the same section uninterpreted (their fig. 15), which is remarkable for the clarity of reflections from the fault plane and from the beds within the hanging wall. Note that their interpretation includes numerous sub-parallel small faults in the hanging wall, thus also establishing a likely directon of simple shear ($\alpha = -15°$). Thus F, B and α are all indicated. Is this interpretation self-consistent?

No stratigraphy was given with this example, and therefore the most difficult parameter to estimate is the heave, h. In the absence of any other information we assume that the top marked reflector, A, is offset from the surface, and that the heave is h, as marked in Fig. 7(b). Since the surface is not horizontal we assume an initial dip of $\gamma_0 = 4°$. θ_0 is estimated as 55°. Three calculated fault shapes are shown in Fig. 7(b), with values of α of -15, 45 and 90°. Clearly, that of 45° agrees best with the observed fault shape, and the value of $-15°$ implied by Wernicke & Burchfiel's interpretation of minor faulting in the hanging wall leads to a poor prediction of the fault shape.

On the face of it a better interpretation would include minor faulting dipping at 45° towards the main fault plane. This is compatible with the uninterpreted observed seismogram, which simply shows severe internal deformation of this part of the hanging wall. In reality of course, with no stratigraphic control on the heave and no corrections for compaction (which may be important, given the obvious growth across the fault and the high deposition rates implied by the non-horizontal surface) or non-uniform vertical exaggeration, this example serves mainly to illustrate the use of the method in testing structural models.

Use of redundant data

It is apparent from the first two examples that the main obstacle to determining the shape of the fault plane

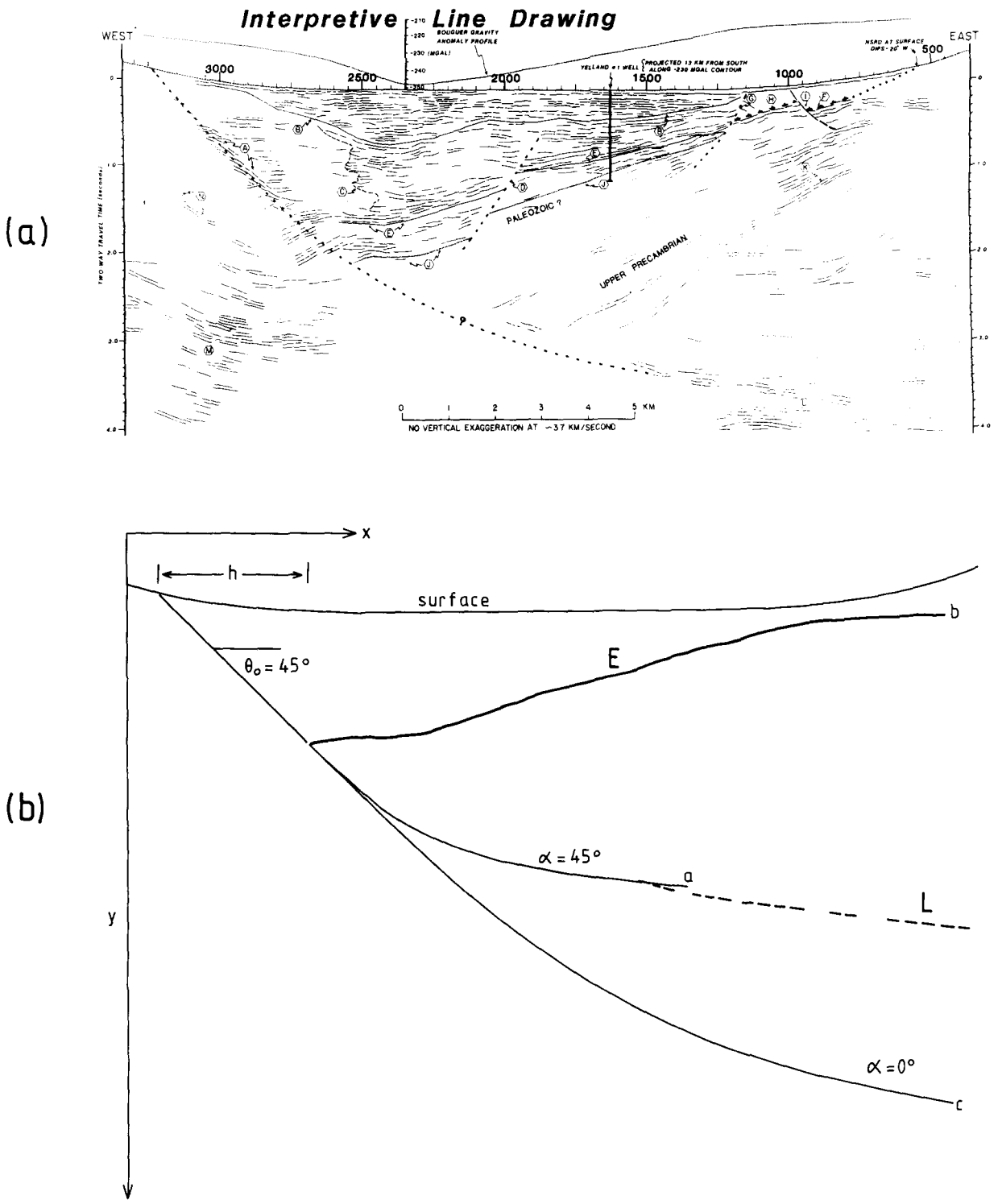

Fig. 6. (a) Line drawing across Spring Valley, east-central Nevada, taken from Gans *et al.* (1985). (b) Shapes predicted for the Schell Creek Fault from the geometry of reflector E shown as lines a (α = 45°) and c (α = 0°). Note that when α = 45° the easternmost point of reflector E contains no information on the fault geometry beyond point a. The position of reflectors L in part (a) are shown by dashed lines in part (b). Both figures have the same horizontal and vertical scales, with no substantial vertical exaggeration in the top part of the section. The values of θ_0 and α are thus approximately true. Reproduced by permission.

(even if depth-corrected, decompacted sections are available) is the unknown direction of simple shear, α. With one observation (B) and two unknowns (F and α) the problem is indeterminate. What progress may be made if the geometry of more than one bed is observable?

Simple shear in the hanging wall is likely to be accommodated by pervasive sub-parallel small faults. Numerous observations suggest that it is easier to continue using an existing fault than to create a new fault, even if the applied stress changes slightly. For this reason the anisotropy or 'grain' imparted to the hanging wall by small faults taking up an early episode of simple shear may well control the direction of simple shear during the

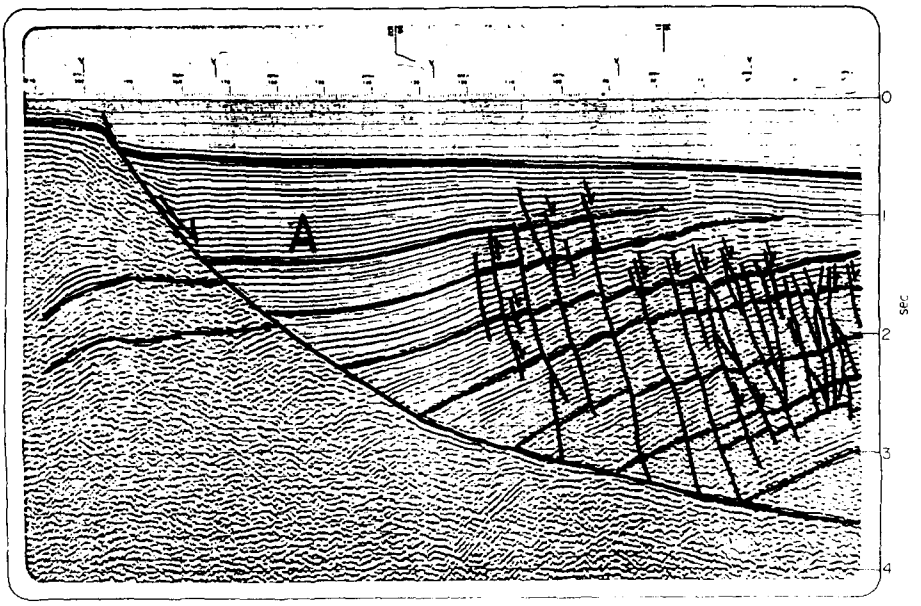

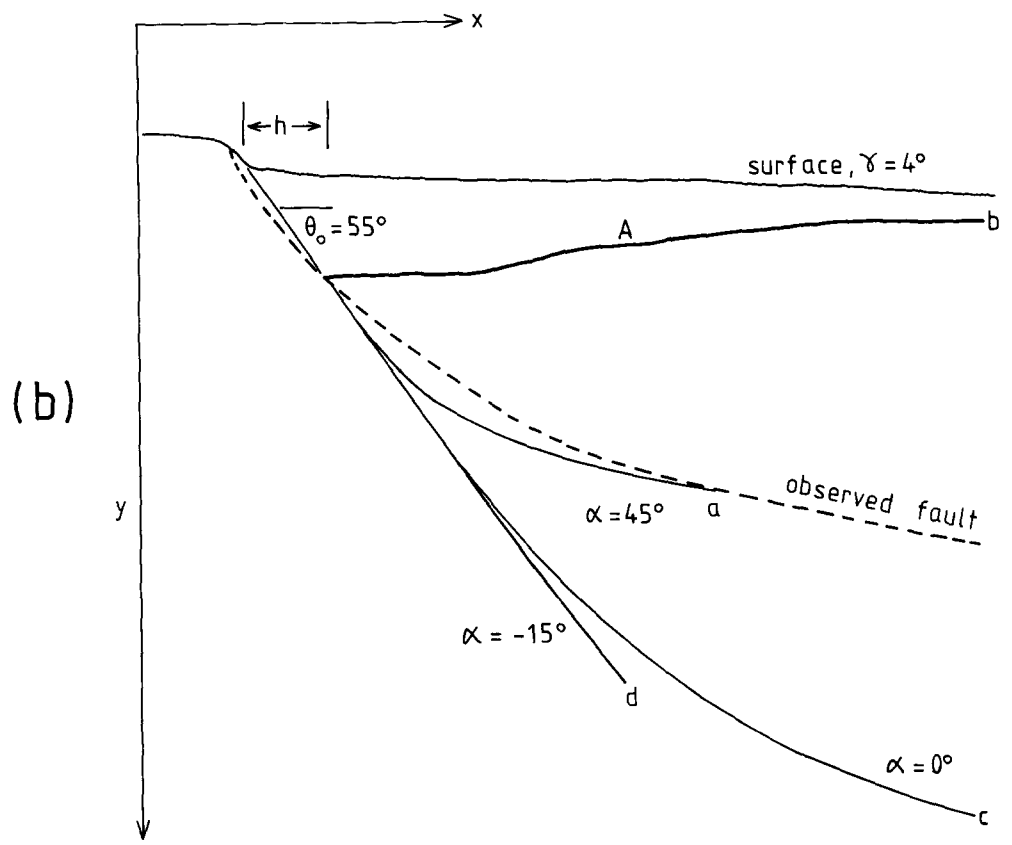

Fig. 7. (a) Interpreted section taken from Wernicke & Burchfiel (1982). (b) Fault shapes predicted from the geometry of bed A using three values of α: -15, 0 and 45°. The vertical and horizontal scales in (a) and (b) are equal. The observed fault is shown by a dashed line in (b). Note that the extent of bed A provides no information on the fault beyond point a when $\alpha = 45°$. For the case of $\alpha = -15°$ the fault extends belows point d, but has been prematurely truncated in this picture. No horizontal scale was given in the original picture of Wernicke & Burchfiel, so vertical exaggeration is uncertain. Reproduced by permission.

subsequent deformation of later, overlying horizons. If this happens, the small faults in the hanging wall will be subparallel at all stratigraphic levels. Since the deformation of the hanging wall is assumed to be by simple shear only, the planes of simple shear are not rotated in the (x', y') frame of the footwall during deformation. Hence, α should remain constant throughout the deformation of the hanging wall. Since the fault geometry also remains unchanged, observations of two bed geometries should be sufficient to determine the two unknowns F and α. With three or more bed geometries known, the assumption of constant α can be tested, and a formal

inversion scheme applied to find the 'best' fault geometry and direction of α which will allow simultaneous fitting of all observed beds. Such a scheme requires both the initial shape, R, of each bed and the displacement on the fault to be known, as there is no reason why they should be the same for different beds.

This approach is illustrated using a section from Bruce (1973; his fig. 7) taken from the Texas coastal area (Fig. 8a). The vertical exaggeration on this section is about 2:1. Is it possible to find a single fault geometry and angle of simple shear, α, that can account for the geometry of both beds A and B? Figures 8(b) and (c) show that the fault geometry suggested by Bruce in Fig. 8(a) can be predicted from both beds, using a common value for α of 26° (true dip 45°), in reasonable agreement with the small hanging wall faults in Fig. 8(a), with $\gamma_0 = 6°$ (true dip 3°) for bed A and $\gamma_0 = 17°$ (true dip 8°) for bed B. These differing values of γ_0 imply that R is not the same for both beds, though their actual values are not dips because of the vertical exaggeration. Note how a value of $\alpha = 0°$ predicts a fault geometry completely different from that suggested by Bruce (Fig. 8d). Once again, since no allowance has been made for variable vertical exaggeration, migration or compaction, this example should be regarded simply as illustrative of the method.

EXTRAPOLATION TO CRUSTAL SCALES

The method of relating fault and sediment geometries described here relies on the footwall remaining undeformed throughout. These ideas are likely to work reasonably well for faults which redistribute the sedimentary cover in a basin, rather than contribute to overall crustal extension. On a crustal scale, where faults penetrate the deep basement and do lead to crustal extension, there are likely to be two difficulties.

The first is that the deeper part of the footwall is likely to experience some form of distributed deformation. This is particularly probable below the maximum depth at which earthquakes nucleate (usually 6–15 km on continents), where, although 'faults' are thought to exist and are seen on some deep reflection profiles, how much motion is concentrated on them and how much is distributed in the blocks either side is unknown. This is discussed further by Jackson (1986). In spite of the uncertainty surrounding the nature of faults in the lower crust, large faults in the upper crust, above the nucleation depths of earthquakes, probably do represent concentrated simple shear with relatively little internal deformation of the footwall. The justification for this statement comes mainly from seismological observations: while aftershocks of major normal faulting earthquakes are common in footwall blocks, their cumulative seismic moment is usually insignificant compared to that of the mainshock. Thus the methods described in this paper should work in the upper parts of large crustal-scale normal faults.

In practice a second difficulty arises: that of large-scale

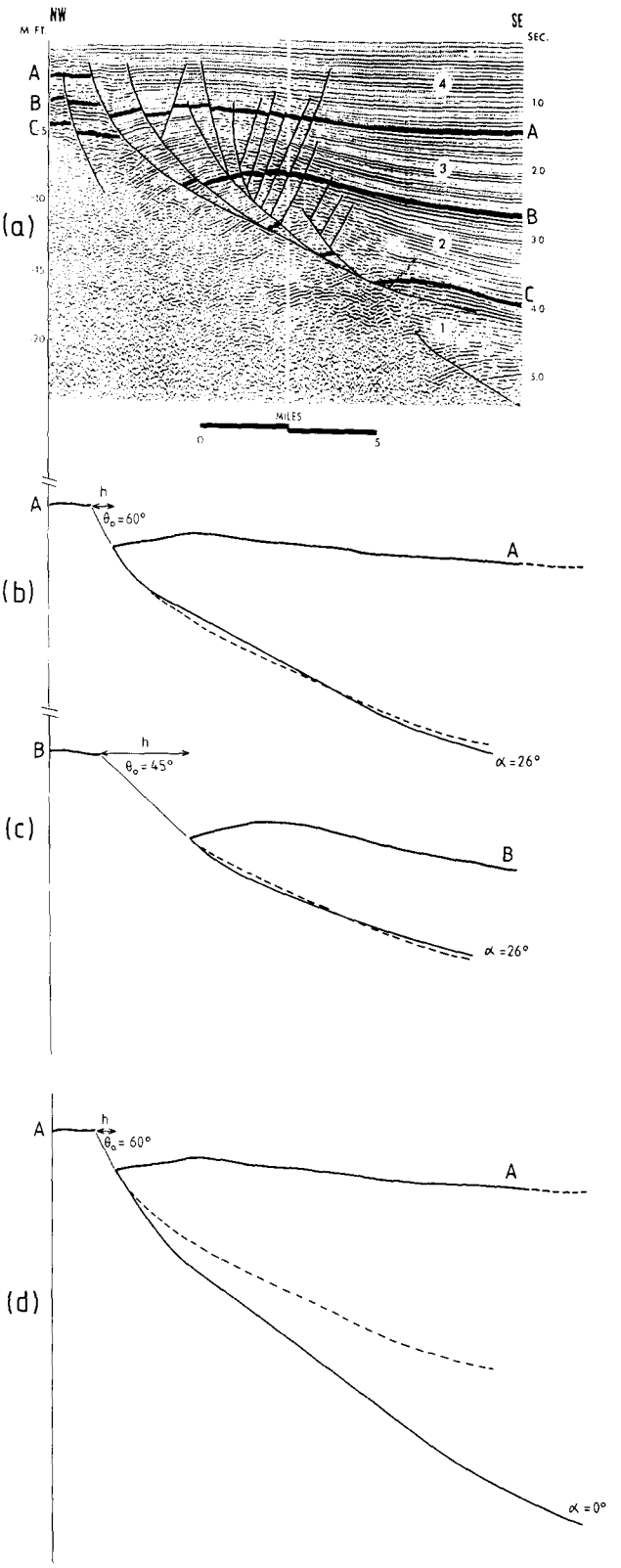

Fig. 8. (a) Interpreted section taken from Bruce (1973). (b)–(d) are drawn with the same vertical and horizontal scales as (a), and show the fault geometries predicted from the shapes of beds A and B using $\alpha = 26°$ (b and c) and $\alpha = 0°$ (d). The fault drawn by Bruce in (a) is shown dashed in (b)–(d). The vertical scale is exaggerated by about a factor of two. Reproduced by permission.

rotation of crustal blocks about a horizontal axis. This is a necessary consequence of trying to stretch the crust (pure shear) by movement on faults (simple shear) and is the justification behind 'domino-style' models of crus-

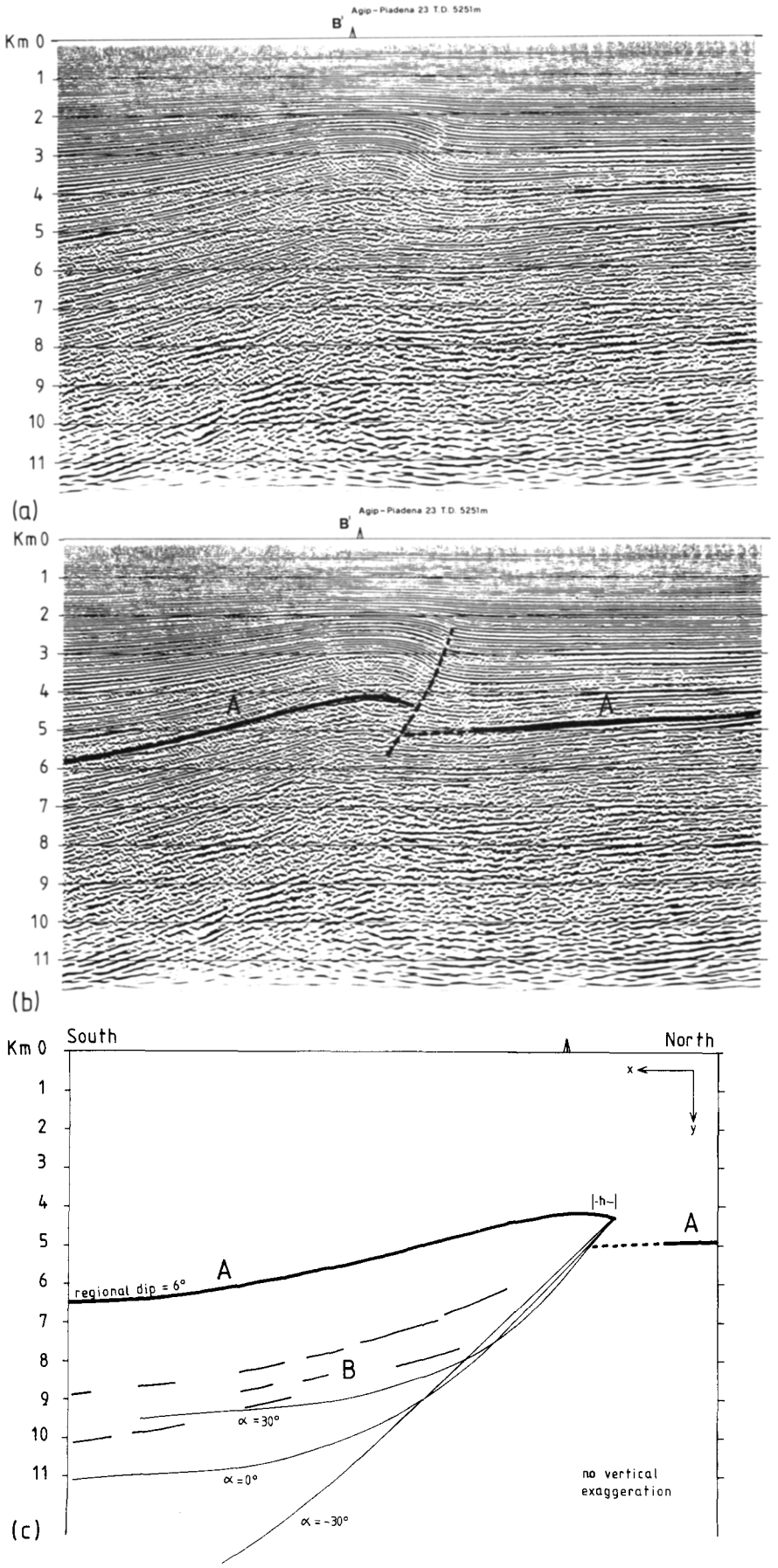

Fig. 9. (a) Migrated and depth corrected seismic section across the Po Plain, Italy, from Peri (1983). The horizontal and vertical scales are equal. (b) and (c) are drawn to the same scale as (a). (b) shows the interpreted position of reflector A, identified as near the top of the Miocene. It is offset by a small thrust fault. (c) Predicted geometry of the thrust with depth calculated from the shape of reflector A, with $\theta_0 = 40°$ and $\gamma_0 = 6°$. Some deeper reflectors, labelled B, are also shown. Three different predicted fault geometries are shown, corresponding to values of α of $-30°$, $0°$ and $+30°$. Reproduced by permission.

tal extension (e.g. Ransome *et al.* 1910, Morton & Black 1975). The rate of this rotation can be calculated if the rate of horizontal extension and the fault block geometry are known (see e.g. Le Pichon & Sibuet 1981; Wernicke & Burchfiel 1982), or can be estimated from stratigraphic arguments. Such rotation means that the footwall itself rotates, and allowance must be made for this when applying the methods used in previous sections.

A NOTE ON THRUST FAULTS

Equations (6) and (11) are equally valid if h is negative and shortening across a thrust fault occurs. The forward problem, of calculating the bed shape given the fault, can be illustrated using the geometry in Fig. 5. Given a bed whose initial shape is $R = h/(1 + x^2)$ and a fault $F = \tan^{-1} x$, what will be the shape of the bed after a small reverse displacement of heave $-h$ on the fault, assuming vertical simple shear ($\alpha = 0°$)?

From (6):

$$B = -h \frac{\mathrm{d}}{\mathrm{d}x} (\tan^{-1} x) + \frac{h}{1 + x^2} + C$$

or

$$B = \text{constant}$$

as it should.

A real example is provided by Peri (1983) in the Po Plain, N. Italy (his fig. 3.4.1–18). Figures 9(a) and (b) show a migrated, depth-corrected seismic section across a thrust that offsets a horizon labelled A, identified from a borehole as near the top of the Miocene sedimentary section. Figure 9(c), which extends a little further south of Figs. 9(a) and (b), shows the geometry of reflector A and also that of some deeper subparallel reflectors, labelled B. The question may be asked: at what depth (if any) does the thrust fault become parallel to the sedimentary layering?

The answer, of course, depends on the inclination of the simple shear that has led to the formation of the gentle fold in the hanging wall. In Fig. 9(c) three different predicted fault shapes are shown, corresponding to values of α of $-30°$ (pervasive imbricate thrusting in the hanging wall), 0° (vertical simple shear) and $+30°$ (pervasive back-thrusting in the hanging wall). In this case no reflectors appear to be continuous across the base of the section, even at the deepest levels, so that perhaps $\alpha < 0°$ (imbricate thrusting) is the most likely. In practice, it is harder to estimate h and θ_0 for thrusts as, unlike in the case of normal faults, abrupt truncations of sedimentary horizons are rarely seen. Figure 9 should therefore be considered only as illustrative of the technique as applied to thrusts.

DISCUSSION

The examples shown here demonstrate that fault shapes can be predicted with some confidence if the direction of simple shear in the hanging wall is known. The assumption that the hanging wall deforms by simple shear is, of course, central to the derivation of the equations we use. This assumption may not be unrealistic, as it is equivalent to implying that the hanging wall deforms by motion on numerous parallel small faults that do not intersect (of the type illustrated in Fig. 7a). All the examples shown here suggest that this simple shear did not occur on vertical planes, but on planes whose true dip is inclined towards the fault at about 45°. This is consistent with the observation that antithetic faults in hanging walls are rarely vertical, even on the scale of faults that penetrate the entire brittle upper crust and generate earthquakes (see Jackson 1986). A dip of 45° is in the middle of the range of dips observed for seismically active normal faults worldwide, and in the absence of any other information it is probably sensible to assume that $\alpha = 45°$ (true dip) rather than 0° [the value used by Verrall (1981) and Gibbs (1983, 1984)]. Such a difference in the value of α leads not only to a great difference in predicted fault shapes (see Figs. 6–8) but also to a substantial difference in the estimated horizontal extension in the hanging wall. Assuming the faults eventually become horizontal at depth, then simple shear inclined at 45° leads to extensions of $2h$ for horizon E in Fig. 6 and $4h$ for horizon A in Fig. 8: increases of 100 and 300% above that estimated from offset of the bed on the fault alone. In the case of thrust faults, ignoring the presence of inclined simple shear will lead to an underestimate of the amount of shortening in the hanging wall.

Compaction may be an additional complication particularly for normal faults. Its principal effects are discussed in the Appendix. Allowing for compaction will not alter the arguments presented in the main body of this paper concerning the importance of inclined simple shear. However one important observation, summarized in Fig. 10(b), is that differential compaction can lead to a pronounced downwarping of sediments in the hanging wall. This may result in the formation of a 'hanging wall syncline', giving the appearance of 'normal drag' with a long wavelength.

If such hanging wall synclines are used to calculate fault geometry without allowing for compaction, the predicted fault will have a convex-upwards shape (Fig. 11), whereas in fact the syncline is more likely to be due to differential compaction of hanging wall sediments above a planar fault.

CONCLUSIONS

Provided displacements are small and the hanging wall deforms by simple shear (thus preserving cross-sectional area), an analytical expression exists that relates the shape of a normal fault in cross-section to the shape of the bedding horizons in its hanging wall block. The expression also assumes that the footwall remains undeformed throughout. The expression may be integrated provided the boundary conditions are specified.

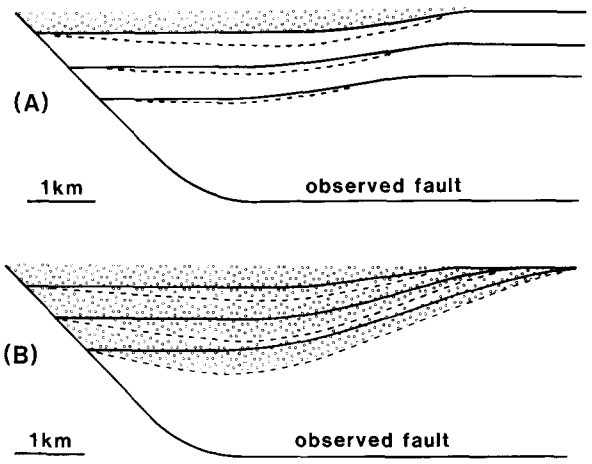

Fig. 10. Bed geometries have been calculated for a given fault with compaction effects taken into account. Solid lines show beds without compaction while dashed lines show beds with compaction. (A) Beds represented by solid lines were deposited, and thus partially compacted, prior to faulting. Motion on the fault causes a depression to form in the hanging wall. This fills with sediment (dotted) causing the original beds to compact further. Note that the deepest bed compacts less than the shallowest one since it was already partially compacted. $\alpha = 45°$, $\phi_0 = 0.6$, $\lambda = 2$ km. (B) All of the beds shown were deposited during faulting. After each increment of slip, the depression formed fills with sediment causing deeper beds, which were originally at the surface, to compact. Note that in (B) the effect of compaction increases with depth whereas in (A) it decreases with depth.

Perhaps the most important result is that the direction of simple shear within the hanging wall block has a very strong influence on the shape of the bedding horizons within it. Graphical techniques relating fault and sediment geometries have been described by Verrall (1981) and Gibbs (1983, 1984), which assume that the simple shear occurs by movement in vertical planes. This condition is clearly a special case, and the examples described here, as well as the observation that minor hanging wall faults are not always vertical, suggests it is not, in general, valid. A substantially different geometry is obtained for the fault if the simple shear planes in the hanging wall are inclined to the vertical, and estimates of the amount of extension in the hanging wall may change by a factor of two or more. Indeed, this study demonstrates that the amount of horizontal extension across a normal fault cannot be estimated simply from the apparent offset of a bed on the fault, if the bed has been deformed in the hanging wall: the dip of the simple shear planes in the hanging wall must also be known.

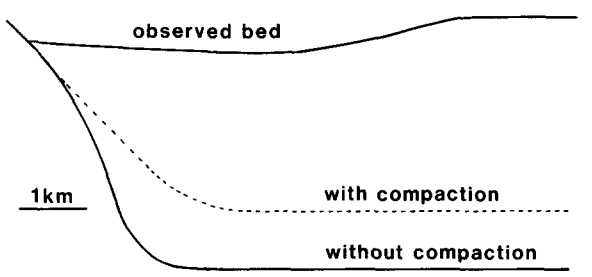

Fig. 11. Illustration of the inverse problem where the fault geometry is calculated given a compacted bed geometry. Solid line shows the fault calculated when compaction is neglected. Note the convex-upwards bulge close to where the bed meets the fault in this case. Dashed line shows the fault geometry obtained with compaction taken into account. Here the upper part of the fault is planar. Parameters as in Fig. 10.

Although this study has concentrated on normal faulting, the method is equally applicable to thrust and reverse faults, as demonstrated by Fig. 9.

Acknowledgements—We thank Peter Verrall for first drawing our attention to this problem at a lecture he gave for the Joint Association for Petroleum Exploration Courses (JAPEC) in London, and D. I. Rainey for many stimulating discussions. Comments made at an early stage by Graham Yielding were very helpful. This work was supported by NERC. N.J.W. gratefully acknowledges a British Council F.C.O. studentship and generous support from Merlin Profilers Ltd. Cambridge University Department of Earth Sciences contribution no. 712.

REFERENCES

Anderson, R. E., Zoback, M. L. & Thompson, G. A. 1983. Implications of selected subsurface data on the structural form and evolution of some basins in the northern Basin and Range Province, Nevada and Utah. *Bull. geol. Soc. Am.* **94**, 1055–1972.

Bruce, C. H. 1973. Pressured shale and related deformation: Mechanism for development of regional contemporaneous faults. *Bull. Am. Ass. Petrol. Geol.* **57**, 878–886.

De Charpal, O., Guennoc, P., Montadert, L. & Roberts, D. G. 1978. Rifting, crustal attenuation and subsidence in the Bay of Biscay. *Nature (Lond.)* **275**, 706–711.

Dahlstrom, C. D. A. 1969. Balanced cross-sections. *Can. J. Earth Sci.* **6**, 743–757.

Gans, P. B., Miller, E. L., McCarthy, J. & Ouldcott, M. L. 1985. Tertiary extensional faulting and evolving ductile–brittle transition zones in the northern Snake Range and vicinity: new insights from seismic data. *Geology* **13**, 189–193.

Gibbs, A. D. 1983. Balanced cross-section construction from seismic sections in areas of extensional tectonics. *J. Struct. Geol.* **5**, 153–160.

Gibbs, A. D. 1984. Structural evolution of extensional basin margins. *J. geol. Soc. Lond.* **141**, 609–620.

Hamblin, W. K. 1965. Origin of "reverse drag" on the downthrown side of normal faults. *Bull. geol. Soc. Am.* **76**, 1145–1164.

Hobbs, B. E., Means, W. D. & Williams, P. F. 1976. *An Outline of Structural Geology*. John Wiley, New York.

Jackson, J. A. 1986. Active normal faulting and crustal extension. In: *Continental Extension Tectonics. Geol. Soc. Lond, Spec. Publs* in press.

Jackson, J. A. & McKenzie, D. P. 1983. The geometrical evolution of normal fault systems. *J. Struct. Geol.* **5**, 471–482.

Le Pichon, X. & Sibuet, J. C. 1981. Passive margins: a model of formation. *J. geophys. Res.* **86**, 3708–3721.

Magara, K. 1978. *Compaction and Fluid Migration, Devs. petrol. Sci.* **9**, Elsevier, New York.

McKenzie, D. P. 1984. The generation and compaction of partial melts. *J. Petrology* **25**, 713–765.

Morton, W. H. & Black, R. 1975. Crustal attenuation in Afar. In: *Afar Depression of Ethiopia* (edited by: Pilger, A. & Rosler, A.) Interunion commission on Geodynamics, Sci. Rep. No. 14. E. Schweizerbart'sche Verlagsbuchhandlung, Stuttgart, 55–65.

Ransome, F. L., Emmons, W. H. & Garrey, G. H. 1910. Geology and ore deposits of the Bullfrog district, Nevada. *Bull. U.S. Geol. Surv.* **407**, 130 pp.

Peri, M. 1983. Three seismic profiles through the Po plain. In: *Seismic Expression of Structural Styles* (Edited by: Bally, A. W.), *Bull. Am. Ass. Petrol. Geol*, Studies in Geology Series No. 15, **3**, 3.4.1–8-19.

Sclater, J. G. & Christie, P. A. F. 1980. Continental stretching: an explanation of the post mid-Cretaceous subsidence of the Central North Sea basin. *J. geophys. Res.* **85**, 3711–3739.

Smith, R. B. & Bruhn, R. L. 1984. Intraplate extensional tectonics of the eastern Basin-Range: inferences on structural style from seismic reflection data, regional tectonics and thermal–mechanical models of brittle–ductile deformation. *J. geophys. Res.* **89**, 5733–5672.

Steckler, M. S. & Watts, A. B. 1978. Subsidence of the Atlantic margin of New York. *Earth Planet. Sci. Lett.* **41**, 1–13.

Verrall, P. 1981. Structural interpretation with application to North Sea problems. Course notes No. 3, Joint Ass. for Petroleum Exploration Courses (UK).

Wernicke, B. & Burchfiel, B. C. 1982. Modes of extensional tectonics. *J. Struct. Geol.* **4**, 105–115.
Wood, R. & Barton, P. 1983. Crustal thinning and subsidence in the North Sea. *Nature (Lond.)* **302**, 134–136.
Ziegler, P. 1983. Crustal thinning and subsidence in the North Sea. *Nature (Lond.)* **304**, 561.

APPENDIX

Unconsolidated sediments generally contain considerable amounts of water (often at least 50% by volume). During burial, this water is lost and the sediment compacts. Such a process will obviously change the shape of a sedimentary horizon within the hanging wall of a normal fault.

The purpose of this appendix is to investigate the importance of this process using expressions which are approximately correct and which should be adequate to illustrate the effects one should expect. Most authors assume that the strain produced by compaction is uniaxial, the axis of shortening being vertical. This assumption is reasonable provided lateral variations in facies and thickness of the sedimentary layers can be neglected. However, it is unlikely to be an accurate description of the strain field in regions undergoing tectonic deformation during sedimentation. The equations governing the behaviour of such a system have recently been developed (McKenzie 1984). Unfortunately they are not easily solved. The principal difficulty is that the compaction rate of the matrix is governed by the pressure of the interstitial water, which is in turn controlled by the water flow within the whole region. Hence local changes in porosity are governed by the behaviour of the whole system. Under these conditions, the porosity cannot be obtained from depth of burial alone.

No attempt has been made here to solve this more general problem. Instead, we have simply modified the standard expressions relating porosity to depth of burial (Magara 1978, Steckler & Watts 1978, Sclater & Christie 1980) so that some of the geometric consequences of compaction can be explored. The resulting eqn (A15) only provides an approximate solution to the full problem and, for this reason, should be applied with care.

Equations developed earlier assume that the hanging wall deforms by simple shear alone. If the strain rate distribution is more complicated, these equations do not hold. This situation is avoided by constraining the strain field produced by compaction to be uniaxial with the axis of shortening parallel to the shear direction within the hanging wall. Under these conditions, the deformation caused by compaction can be treated separately to that caused by movement on the fault. Hence the problem can be solved. It is important to stress that the above constraint has been arbitrarily imposed so that a solution may be obtained with ease. Nevertheless it is unlikely to be any worse than assuming that compaction involves uniaxial shortening which is purely vertical.

The necessary expressions may now be derived. Given that compaction occurs by uniaxial shortening parallel to y', the resultant velocity field is calculated. This is required to be parallel to the fault at every point so that voids do not form at depth. The final result is a first-order differential equation which can be solved by iteration.

The porosity at any depth, d, below a pre-faulting surface of dip γ is

$$\phi = \phi_0 \exp\left\{-\frac{d}{\lambda}\right\} \tag{A1}$$

where

$$d = y - x \tan \gamma, \tag{A2}$$

ϕ_0 is the initial porosity and λ is a constant governing the change of porosity with depth. As before, the (x', y') co-ordinate frame is rotated through an angle, α, with respect to the (x, y) frame. Therefore the porosity at any point in the (x', y') frame is

$$\phi' = \phi_0' \exp\left\{-\frac{y'}{\lambda'}\right\}, \tag{A3}$$

where

$$\phi_0' = \phi_0 \exp\left\{-\frac{x' \sin(\alpha - \gamma)}{\lambda \cos \gamma}\right\} \tag{A4}$$

and

$$\lambda' = \frac{\lambda \cos \gamma}{\cos(\alpha - \gamma)}. \tag{A5}$$

As before, the fault, $F'(x')$, is considered fixed in the (x', y') co-ordinate frame. We determine the movement of the bed, given by $B'(x_0', t)$ where x_0' is the initial value of x' for some point on the bed. A Lagrangian reference frame x_0' is then used to follow the movement of a point on the bed. By differentiating with x_0' fixed, the velocities in the x' and y' directions are

$$U_0 = \left(\frac{\partial x'}{\partial t}\right)_{x_0'}, \qquad v = \left(\frac{\partial B'}{\partial t}\right)_{x_0'}, \tag{A6}$$

respectively. Neither $F'(x')$ nor $\phi_0'(x')$ are functions of t in the (x', y') frame. Differentiation of $F'(x')$ thus gives

$$\mathrm{d}F' = \frac{\mathrm{d}F'}{\mathrm{d}x'}\,\mathrm{d}x'.$$

Therefore

$$\left(\frac{\partial F'}{\partial t}\right)_{x_0'} = U_0 \frac{\mathrm{d}F'}{\mathrm{d}x'} \tag{A7}$$

similarly

$$\left(\frac{\partial \phi_0'}{\partial t}\right)_{x_0'} = U_0 \frac{\mathrm{d}\phi_0'}{\mathrm{d}x'}, \tag{A8}$$

where U_0 is the x' component of the velocity (constant within the hanging wall).

Both (A7) and (A8) take account of the effect of compaction on the velocity field.

The volume of solid material, V_s, in a vertical section between the bed and the fault is

$$V_s = \int_{B'}^{F'} (1 - \phi')\,\mathrm{d}y'. \tag{A9}$$

Substitution of (A3) into (A9), followed by integration yields

$$V_s = F' - B' + \phi_0' \lambda' \left\{\exp\left(-\frac{F'}{\lambda'}\right) - \exp\left(-\frac{B'}{\lambda'}\right)\right\} \tag{A10}$$

Since compaction is uniaxial in the y' direction, V_s must remain constant in a frame fixed to the hanging wall. Therefore

$$\left(\frac{\partial V_s}{\partial t}\right)_{x_0'} = 0. \tag{A11}$$

Note that the condition

$$\frac{\partial V_s}{\partial t} = 0 \tag{A12}$$

is not satisfied because in a frame fixed to (x', y'), and thus to the footwall, the volume of sediment between the bed and the fault at any given value of x', must change as the hanging wall is displaced. In an extreme case, when the hanging wall moves far enough, the point where the bed meets the fault passes the chosen value of x' and there is no material left between the fault and the bed. Clearly conservation of sediment volume only occurs in a frame fixed to the hanging wall (x_0'). Therefore (A11) is the correct condition to impose. Differentiation of (A10) gives

$$\left(\frac{\partial F'}{\partial t}\right)_{x_0'} - \left(\frac{\partial B'}{\partial t}\right)_{x_0'} - \phi_0'\left\{\left(\frac{\partial F'}{\partial t}\right)_{x_0'} \exp\left(-\frac{F'}{\lambda'}\right) - \left(\frac{\partial B'}{\partial t}\right)_{x_0'} \exp\left(-\frac{B'}{\lambda'}\right)\right\} + \left(\frac{\partial \phi_0'}{\partial t}\right)_{x_0'} \lambda' \left\{\exp\left(-\frac{F'}{\lambda'}\right) - \exp\left(-\frac{B'}{\lambda'}\right)\right\} = 0. \tag{A13}$$

As before, movement should be parallel to the fault. This gives, from (6),

$$v\,\delta t = B' - R' - C', \qquad U_0\,\delta t = h'. \tag{A14}$$

Substitution of (A4), (A6), (A7), (A8) and (A14) into (A13) then yields

$$\frac{\mathrm{d}F'}{\mathrm{d}x'} = \frac{(B' - R' - C')\{1 - \phi_0' \exp(-B'/\lambda')\}}{h'\{1 - \phi_0' \exp(-F'/\lambda')\}} - \frac{\phi_0' \tan(\alpha - \gamma)\{\exp(-B'/\lambda') - \exp(-F'/\lambda')\}}{\{1 - \phi_0' \exp(-F'/\lambda')\}}. \tag{A15}$$

This first-order differential equation can be solved by iteration either for F' when B' is given, or for B' when F' is given. When $\phi_0' = 0$, (A15) reduces to a previously derived expression. This provides an initial solution to (A15). Only three or four iterations are then required to find the correct solution since convergence is rapid.

Examples and implications

Figure 10 illustrates the effect of compaction on two different depositional situations. In Fig. 10(a) the beds were deposited, and hence partially compacted, prior to the onset of faulting. As a result of faulting, beds close to the fault move to deeper levels than those further away in the hanging wall and are buried by young sediments deposited in the depression adjacent to the fault. Therefore, beds close to the fault compact more than those further away in the hanging wall block. The effect on bed geometry is greater for shallow beds since deeper beds lost much of their porosity prior to faulting.

Figure 10(b) shows the effects of compaction on beds that were all deposited during faulting. In this case compaction leads to a pronounced downwarping of beds adjacent to the fault resulting in the creation of a 'hanging wall syncline'. This is similar in shape to what is often described in the lierature as 'normal drag' (Hamblin 1965, Hobbs *et al.* 1976), except that it is on a longer wavelength.

It is important to note that if such synclines are used to infer fault geometry without allowing for compaction, a convex-upwards fault is predicted (Fig. 11). In fact, it is more likely that hanging wall synclines arise due to differential compaction above an initially planar fault. The presence of features similar to those illustrated in Figs. 10 and 11 is probably a good indication that the effects of compaction are significant and should be allowed for.